Proceedings of the 21st ICSMGE, Vienna, Austria, 14 – 19 June 2026. Pistrol, Adam & Schweiger (eds.)
Published by: ÖGG, Austrian Society for Geomechanics, Salzburg, Austria, ISBN 978-3-9503898-4-5
https://doi.org/10.53243/ICSMGE2026-370

Subsidence effects on the seismic performance of end-bearing piles.

[1*]Juan Manuel Mayoral, [1]Mauricio Pérez, [2]Azucena Román-de la Sancha, and [1]Ingrid Guzmán.
*[1]Institute of Engineering, National Autonomous University of Mexico, Mexico, *jmayoralv@iingen.unam.mx*
[2]School of Engineering and Science, Tecnólogico de Monterrey, Mexico

ABSTRACT: End-bearing piles are often used in high compressible soft soils to support medium to large structures, transmitting the loads to a more competent soil stratum found underneath the soft soil formation. This solution enhances bearing capacity and reduces settlements considerably, nevertheless, when dealing with regional subsidence associated with underground water extraction, leads to structure emersion, negative skin friction around the piles, and pile overloading due to soil dragging. These effects are well stablished, and even several worldwide construction codes provide recommendations for designing piles under these conditions. However, there´s still a lack of understanding on the expected seismic performance during the economic life of the structure as the consolidation evolves. This paper presents a numerical study on the expected impact on the dynamic behavior of a 3 by 3 array, end-bearing piles foundation of a bridge support, when considering a variable soil foundation depth, for scenarios at 0, 15, 25 and 50 years in a site located in Mexico City clays. Initially, a three-dimensional model developed with the program FLAC3D of the soil deposit was developed to establish ground settlement evolution at the studied area. Thus, the presence of the structure was included in the simulation. Once the static conditions were determined for each scenario, series of three-dimensional finite difference models of the bridge support system were developed, and the response for each scenario was considered for the 2017 Puebla-Mexico earthquakes. From the results gathered here the expected change in the dynamic behavior of bridge, and structural demand on foundation elements were established.

KEYWORDS: regional subsidence, end-bearing pile foundations, soft soil and soil-structure interaction.

1 INTRODUCTION

End-bearing piles play a critical role in supporting loads and controlling settlement under static conditions (e.g., Firoj & Maheshwari, 2022). In seismic regions, however, their performance is equally vital due to dynamic soil–structure interaction (SSI), which significantly affects structural stiffness, damping, and its natural frequency of vibration (e.g., Zhao et al., 2017). Despite growing awareness, fully coupled SSI seismic design remains a challenge due to modeling and code complexities (e.g., Mital & Samanta, 2024).

Simultaneously, urban areas like Mexico City face severe regional subsidence from groundwater over-extraction, modifying effective stress and soil behavior. For deep foundations, this stress change can induce negative skin friction, increasing axial loads prior to seismic events (O'Riordan et al., 2018). Over time, subsidence may disturb soil properties around piles, a factor often overlooked in seismic design. Past earthquakes (e.g., Kobe, Loma Prieta) have highlighted the risk of neglecting SSI (e.g., Barbosa et al., 2014), a concern exacerbated in subsiding regions. This study aims to investigate these interrelated phenomena, providing essential insights into the complex behavior and seismic vulnerability of structures founded on end-bearing piles in environments characterized by significant regional subsidence.

2 METHODOLOGY

Due to the complex characteristics of the studied case, particularly the interplay of modeling subsidence and its seismic soil-structure interaction, a comprehensive direct approach was adopted. This rigorous method, adopted to detailly address SSI problems in areas affected by regional subsidence like Mexico City, involves the modeling of the soil and structure as a single, integrated system. The implemented methodology proceeds in four key steps. First, all input parameters are defined, including detailed information about the structure, foundation, soil properties, the dynamics of pore pressure evolution, subsidence rates, and the governing seismic environment. Second, the soil elements are modeled, explicitly simulating subsidence through the reduction of pore pressure, which in turn updates the soil's stiffness. Third, the foundation and structural components are constructed step-by-step to reflect the in-situ construction sequence; afterward, subsidence is applied in each case study, affecting the structural behavior and capacity. Finally, the seismic performance of the bridge is rigorously evaluated by assessing the structure's displacements and internal forces verifying its performance, and crucially, identifying how regional subsidence impacts its overall behavior during seismic events.

3 CASE STUDY

Mexico City, built largely on ancient lakebeds such as Texcoco and Xochimilco-Chalco Lakes, faces significant regional subsidence due to extensive groundwater extraction. Soft lacustrine clay deposits formed from volcanic ash and pyroclastic materials, with thicknesses of 20 to 100 meters are often found around the city basin. Around 66% of the city water supply comes from groundwater, leading to severe aquifer overexploitation, with a supply deficit of nearly 23 m³/s and pore pressure depletion in highly compressible clay layers (Cabral-Cano et al., 2024). This has triggered a consolidation process in the soft lacustrine clays, producing cumulative settlements of up to 10 meters in some areas (Ovando-Shelley, Ossa and Romo, 2007), with sinking rates exceeding 40 cm/year in some zones (RCDF, 2023).

This subsidence profoundly impacts end-bearing pile foundations. As the surrounding ground subsides, piles supported by deeper, stiffer strata appear to "protrude", creating negative skin friction along the pile, and potentially forming gaps underneath footings, which compromise the foundation system's ability to withstand seismic loads (Fig. 1). To address this, the RCDF (2023) mandates designing end-bearing piles as short columns with additional transverse steel reinforcement in the deconfinement zone.

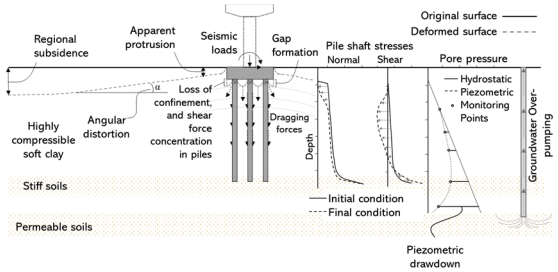

Figure 1. Schematic representation of the end-bearing pile foundation long-term behavior by piezometric drawdown and regional subsidence.

3.1 *Description of the structural system of the bridge*

The studied bridge section corresponds to a typical structure for massive public transport for urban overpasses within the soft lacustrine soil deposits in Mexico City.

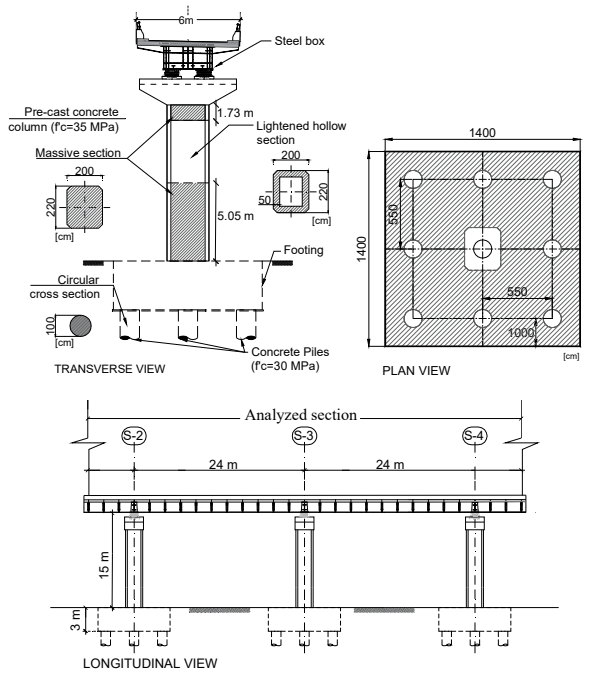

Figure 2. Transverse and longitudinal views of the studied overpass section.

The superstructure consists of a 25 cm-thick reinforced concrete deck supported by a continuous 1.6 m-high steel box girder. This steel box rests on reinforced concrete pier caps, structurally connected to the columns. The pre-cast concrete columns have lightened hollow cross-sections and are seated on massive squared 14 by 14 m^2 footings 3.0 m thick. These footings are connected to 1.0 m-diameter, cast-in-situ, end-bearing piles of 20 m long with a 3x3 array distribution as depicted in figure 2. The compressive strength of the concrete at 28 days was f`c=35 MPa for the columns and footings, and f`c=30 MPa for the piles. Figure 2 provides a schematic view of the bridge's structural system. Illustrating a transverse and plan view of the typical support configuration, highlighting the column's cross-section with both massive and lightened hollow portions, as well as the piles distribution. Lastly, the longitudinal view displays the span lengths, footing depths for each support, and column heights.

3.2 *Subsoil conditions*

According to the geotechnical conditions of the basin, former Mexico City building code classifies the hill and the transition zone as I and II, respectively, while the lake zone has been further subdivided into zones IIIa, IIIb, IIIc and IIId as the thickness of the clay increases. Figure 3 depicts the location of the case study on the former zonation map, which falls in Zone IIIa.

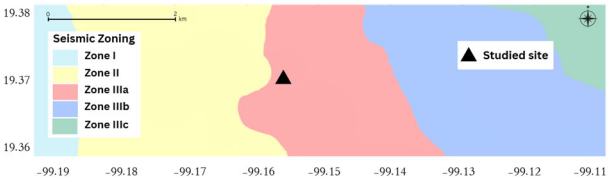

Figure 3. Location of the study site.

The soil profile at the selected site was thoroughly characterized using data from Standard Penetration Tests (SPT) and comprehensive laboratory analyses of recovered undisturbed samples. This profile is primarily defined by a substantial clay layer that occupies the upper 23 meters. Within this dominant clay stratum, the groundwater level was specifically identified at approximately 4.5 meters below the surface. Underneath this extensive clay deposit, the profile transitions into a clayey sand, indicating a shift towards a denser and more permeable stratum at greater depths, where the pile tip foundation is supported. Figure 4 depicts the distribution of the soil strata with the bridge foundation schematical representation, the pore pressure and shear wave velocity distribution with depth. This last one was taken from the measurements made by Wood et al. (2023).

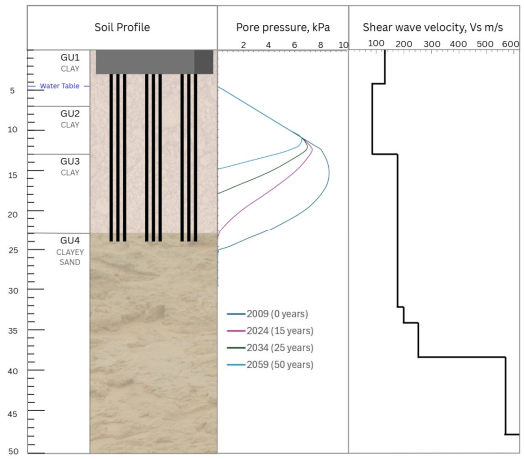

Figure 4. Soil profile, pore pressure distribution for each case analysis and the soil profile of Site 1.

Table 1 details the properties of the soil profile which is divided into four geotechnical units (GU). The upper three units (GU1–GU3) are predominantly soft clays, with varying degrees of compressibility, characteristic of lacustrine deposits. These are underlain by a dense and stiff bearing layer of clayey sand (GU4) extending to 70 meters depth, providing the primary support stratum for foundation design.

Table 1. Soil profile properties.

Unit	D [m]	CM	γ [kN/m³]	PI [%]	Su [kPa]	φ' [°]	E_{50}^{ref} [MPa]	E_{oed}^{ref} [MPa]	E_{ur}^{ref} [MPa]	e0	OCR
GU-1	0-7	HS	12.7	190	31.4	35	350	165	1400	1.6	1.51
GU-2	7-13	HS	10.7	360	34.5	40	160	60	900	3.9	1.39
GU-3	13 -23	HS	11.3	270	76.5	43	170	30	560	5.5	1.12
GU-4	23 -70	MC	17.7	10	4.9	35	4000	-	-	-	-

Where D is depth; CM is constitutive model; γ is the volumetric weight; PI is the plastic index; Su is the undrained shear strength; φ' is the effective friction angle; E_{50} is the secant modulus for triaxial loading conditions; E_{oed} is the oedometric modulus obtained from unidimensional consolidation tests; E_{ur} is the Young's modulus for unloading and reloading in the elastic range; e0 is the void ratio; and OCR is the over consolidation ratio.

3.3 *Pore pressure distribution*

Variation of pore pressure distribution with depth over the years (2009 to 2024) was obtained from piezometric data collected at the site. Based on the measurements, a downward trend was established for each depth to estimate the pore pressure profiles for subsequent study periods, specifically at 25 and 50 years. Figure 4 illustrates the measured and estimated isochrones.

3.4 *Seismic environment*

Mexico City's seismic hazard primarily stems from two sources: shallow (less than 40 km) interface earthquakes from

Cocos and Rivera plate subduction, and deeper (40-460 km) intraplate earthquakes within the subducted Cocos plate (Singh et al., 2018; Zúñiga and Suárez, 2017). Both responsible for the M8.1, 1985 Michoacan and the M7.1, 2017 Puebla earthquakes. The 2017 event mainly affected regions where the fundamental period of vibration of the soil was between 1 to 1.5s (Mayoral, et al., 2017). Seismic energy concentrated within this period band leading to a resonance effect that affected mid- to high-rise structures.

As depicted in Figure 3, the case study is in zone IIIa, where the soil period is approximately 1-1.5s, thus ground motion characteristic of an intraplate earthquake was considered in the analyses. Ground motions recorded by both horizontal components of movement at station CUP5, located on a rock outcrop during the September 2017 earthquake were used as seed ground motions for site analysis (Figure 5).

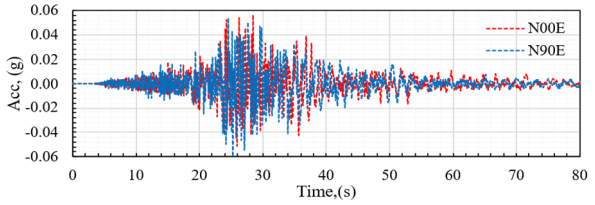

Figure 5. Accelerations time histories recorded by the station CUP5 during the September 19, 2017, Puebla-Mexico earthquake.

Synthetic ground motions were developed so that their 5% damped response spectrum reasonably matches the target design response spectrum, using the method proposed by Lilhanand et al., (1988), and modified by Abrahamson (2000). Two different levels of ground shaking were defined through Probabilistic Seismic Hazard Assessment (PSHA), for return periods of 475 and 1000 years, as in Osorio and Mayoral (2013). The 475-year return period corresponds to a 10% probability of exceedance in 50 years and is widely used in seismic design to represent an infrequent but credible earthquake (FEMA, 2009). This benchmark aligns with the expected service life of standard infrastructure and provides a balanced approach between safety and economy. Additionally, seismic demand was evaluated using risk-targeted ground motions associated with a 1000-year return period, as required for critical and essential infrastructure, in accordance with the AASHTO guidelines (2023). Figure 6 depicts the calculated uniform hazard spectrum, UHS.

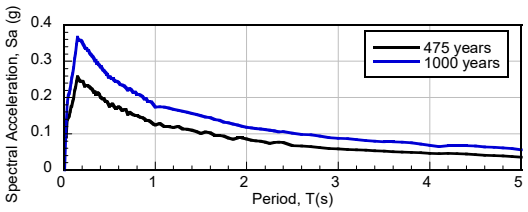

Figure 6. Uniform hazard spectra associated with a return period of 475 and 1000 years.

4 NUMERICAL MODEL

4.1 *Structural modelling*

Structural analyses were performed using three-dimensional finite difference models that captured the geometry, mechanical properties, and interconnectivity of the main structural components (Figure 7). Developed in FLAC3D, the model represented columns, pier caps, and the deck using BEAM and SHELL elements. All materials were assumed to behave linearly elastically, and structural performance was assessed based on internal force limits, and lateral displacements. The mechanical and geometrical parameters of the structural elements are summarized in Table 2.

Table 2. Mechanical and geometrical parameters of the structural elements.

Element	γ (kN/m^3)	A (m^2)	Ix (m^4)	Iy (m^4)	E_s (MPa)	ν [-]
Support* beams	24/78	3.13	1.84	7.73	2.57E+4/ 2.00E+5	0.2/ 0.3
Columns						
Massive	24	8.75	5.33	7.44	2.57E+4	0.2
Hollow	24	4.82	4.33	5.78	2.57E+4	0.2
Massive	24	8.75	5.33	7.44	2.57E+4	0.2
Pier caps	24	6.00	2.00	4.50	2.57E+4	0.2

*Note: These elements are formed by a composed section that considers the steel box and the concrete deck.
Where γ is the volumetric weight; A is the cross-sectional area of the element; Ix and Iy are the moments of inertia about the transverse and longitudinal axis of the element, respectively; f'c is the nominal compression strength of the concrete, fy is the yielding stress of the steel; Es is the Young's modulus of the element; and ν is the Poisson ratio.

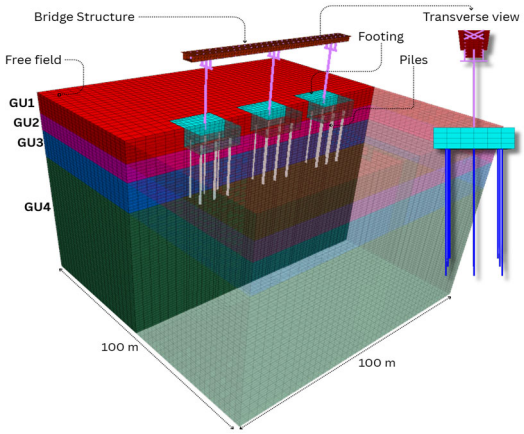

Figure 7. Three-dimensional finite difference model considering the bridge structure and foundation elements.

4.2 *Soil modelling*

The soil–foundation system was modeled in FLAC3D, incorporating soil, footings, and piles. Soil behavior was represented using solid elements and the constitutive model Mohr-Coulomb, MC, for sands, silts, gravels, and fractured rock, and the Hardening-Soil model, HS, (Schanz et al., 1999) for soft clays. Model parameters were calibrated using site-specific laboratory and field test data, with soil properties detailed in Table 1.

Due to the lack of experimental data regarding modulus degradation and damping parameters, the model developed by Darendeli and Stokoe (2001), D&S, where used to generate the corresponding curves for the soft clay, in function of the PI and the effective confinement stress, σ'$_c$. For the clayey sand, the lower bound curves developed for sands by Seed & Idris (1970) was used. The used curves are depicted in Figure 8.

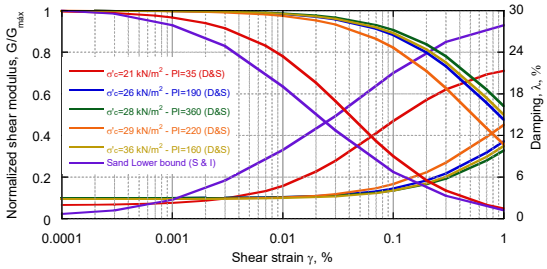

Figure 8. Normalized shear modulus degradation and damping curves for the study.

The boundary conditions of the model's base for dynamic simulations were defined using the Lysmer and Kuhlemeyer's (1969) formulation. In the case of the lateral faces of the model, free-field boundaries were considered using the formulation available in FLAC3D.

4.3 *Simulation of foundation elements*

Foundation piles were modeled in FLAC3D using PILE elements, with spring parameters derived from the surrounding soil in accordance with Yeganeh et al. (2015). Table 3 presents the shear and normal spring parameters. Footing was represented by solid elements with linear-elastic behavior, and all components included interfaces to simulate relative displacements between soil and foundation elements.

Table 3. Summary of the values of the parameters of the pile's shear and normal spring soil mechanical properties.

Unit	cs_{scoh} [kN/m]	cs_{sfric} [°]	cs_{sstiff} [MPa]	cs_{ncoh} [kN/m]	cs_{nfric} [°]	cs_{nstiff} [MPa]
UG-1	3.77	8.75	5805	14.40	11.67	1847
UG-2	12.37	26.25	70144	47.25	35	22327
UG-3	12.44	30.00	32065	47.52	40	10206
UG-4	27.57	32.25	34070	105.30	43	10844

Where c_{soil} and φ_{soil} is the cohesion and internal friction of the soil adjacent to the pile, p is the exposed perimeter of the pile, K an G are the bulk and shear moduli of the adjacent soil, $\triangle z_{min}$ is the smallest width of an adjoining zone in the normal direction, α is a parameter that depends on the condition of the pile surface advising for the rough surface (e.g. cast-in-situ pile) to be equal to 1 and $D_{pile}$is the pile diameter.

4.4 *Simulation of ground subsidence*

Ground subsidence was first modeled under free-field conditions using a soil column defined by key parameters (Table 1) and stratigraphy (Figure 4). Simulations for 2009, 2024, 2034, and 2059 involved withdrawing pore pressure and calculating the corresponding displacements. This method was initially applied to the soil column and then incorporated into the full 3D model. Figure 9 presents the resulting displacements over time.

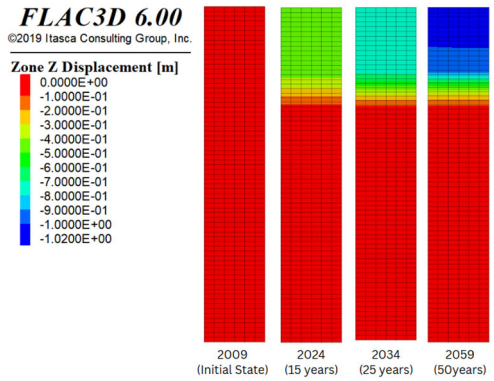

Figure 9. Soil column consolidation simulation.

The analysis excludes ground settlement prior to the first measurement year, focusing instead on settlements occurring from the 2009 condition onward. After calibrating the free-field models, consolidation analyses incorporating structural and foundation systems were conducted for each stage. The final simulation stage yielded maximum vertical displacements of around 1 m.

4.5 *Simulation of seismic site response*

To establish the input motion applied at the base of the model, the surface ground motion was deconvolved with the program SHAKE (Schnabel et al. 1972) and applied as a stress time history according to the compliant base approach (Itasca, 2009).

The accuracy of the model was assessed by comparisons of the computed responses at ground (Figure 10), including the measurement of the seismic station AU46, located at approximately 1.6 km from the studied site in the same geo-seismic zoning (i.e. Zone IIIa). As can be seen, the model is capable of reproducing the amplification of the seismic response adequately.

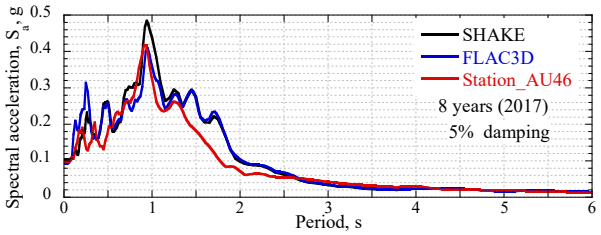

Figure 10. Comparison between calculated study site and measurements (Station AU46).

5 RESULTS

5.1 *Static long-term behavior*

Regional subsidence and differential settlement cause several long-term problems, including significant down-drag forces on piles, detrimental gaps under footings, and surface cracking around structures. While the bridge superstructure maintains stability due to end-bearing piles on stable deeper ground, adjacent infrastructure functionality is disrupted. Critically, the numerical model predicts a separation of 0.66 m between the footing and ground at the final stage as shown in Figure 11, which represents 64% of the free field subsidence. Figure 12 depicts the normal stress contours plot of all the simulated stages at the base of the footing in support S-3, showing almost zero normal stresses by 50 years at the interface element, indicating contact loss in the footing areas. In addition, pile axial force increases due to dragging forces generated as the consolidation increases, nevertheless for the 50 years condition, there is a reduction which can be associated with the shear yielding of the soil-pile interface.

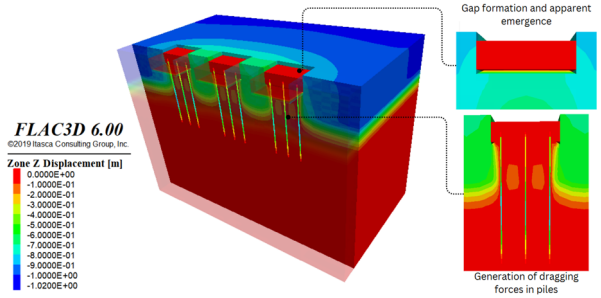

Figure 11. Vertical displacements from the numerical model for the final case of the simulation, showing the different potential problems generated by regional subsidence.

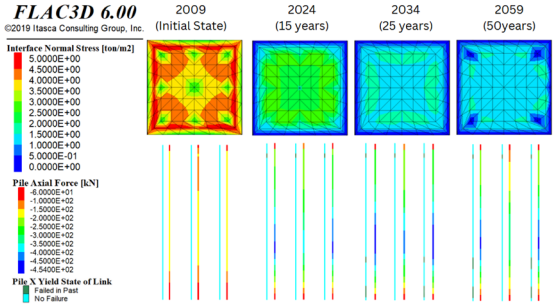

Figure 12. Variation of normal stresses with time at the interface between the footing S-3 and the bearing ground along with the

evolution of axial force in the central piles and the yield state of links between the piles and the soil.

5.2 *Soil-structure interaction effects*

Following the free-field analyses and calibration of the dynamic parameter for ground shaking simulation, the seismic response for the bridge system was carried out considering each subsidence scenario. In accordance with Mayoral et al. (2009), the impact of the seismic motion in the bridge's longitudinal direction is less significant compared to its transverse direction, thus special attention was paid on the transverse response. Figure 13 presents a comparative analysis of the Fourier spectra obtained at bridge's deck for all the consolidation stages. It is evident that the fundamental frequency of vibration of the structure system is approximately 1.4 Hz (0.71 s), where the main amplification of seismic forces occurs in the 0 years scenario. This amplification decreases, and the frequency where the main amplification occurs increases as the consolidation evolves. This can be associated with the loss of contact between the foundation and the soil, which changes drastically the way that the soil interacts with the structure, influencing the structure's overall vibrational response.

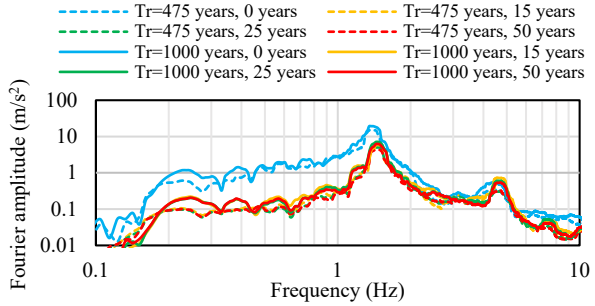

Figure 13. Fourier spectra obtained at the bridge's deck for all the consolidation stages.

To verify the changes in the seismic motion at the base of the footings, the transfer function between that point and the free field was obtained for each consolidation stage (Figure 14). For the 0 years scenario, a clear reduction in the amplitude can be noted for frequencies higher than 4 Hz, which can be associated with the motion uniformity effect due to the kinematic constraint of the footing. Nevertheless, for the following cases where the footing began to lose contact with the soil, the movement seems to decrease for all frequencies. This effect could be associated with the changes in the transfer mechanism of seismic motion between the soil and the foundation, which occur mainly through the piles and lateral faces of the footings, in the consolidated cases.

Due to such changes in the transfer mechanism of the motion, structural demand is expected to be affected for all the consolidation stages.

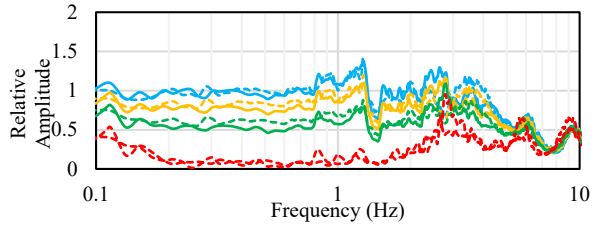

Figure 14. Base foundation/free field transfer functions, for all the consolidation stages.

Figure 15a and 15b shows the bending moment variation during the dynamic simulation, for all consolidation stages, at the column base of the central pier (S-3) and at the pile head of the corner, with plastic moments of 66685 kN-m and 3530 kN-m, respectively. However, due to the order of magnitude difference between the acting and resistant bending moment of the central pier, the latter was not included in the plot. As can be seen, in any consolidation stage the plastic moments were exceeded indicating that no plastic yielding occurred. For the 0 years condition, the seismic load concentrates at the column base, and the structural demand of the pile is almost negligible in comparison to such of the column. Nevertheless, for the following scenarios the bending moment at pile´s head increases in every consolidation stage and decreases at the column's base. These effects are congruent with the transfer mechanism of motion, discussed above. Due to seismic waves rise up into the structure through the piles, those become the main earthquake resistant elements, and then their structural demand increases. In addition, interaction with the soil decreases as the footing-soil contact gets loose, thus the piles are subjected to increased bending moments and shear forces under seismic excitation, as they are forced to resist a larger proportion of the lateral and rotational demands from the superstructure.

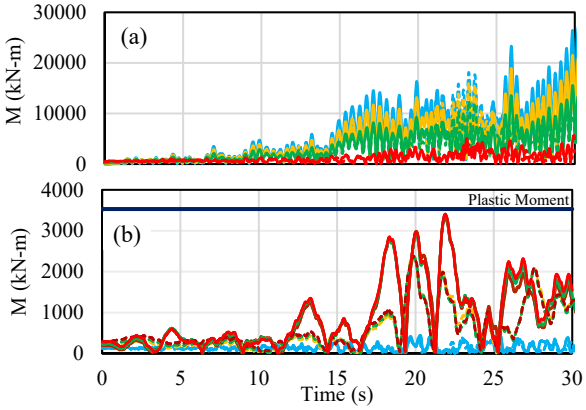

Figure 15. Bending moments during the dynamic simulation for each consolidation stage, (a) at the column's base, and (b) at pile's head.

Considering all the effects discussed above, the following statement can be made: in bridges founded on end bearing piles located on soft soils subjected to regional subsidence, the structural demand of the piles against a seismic event will increase for the long-term condition, and the structural demand will decrease on the pier. Figure 16 depicts the bending moments at the pile's head and at the column's base, for all the consolidation stages normalized with the 0 years condition, which support the above statement.

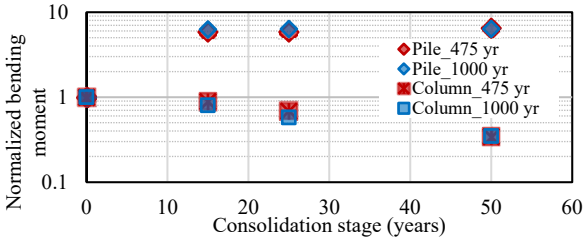

Figure 16. Normalized bending moments during the dynamic simulation for each consolidation stage, (a) at the column base, and (b) at pile head.

6 CONCLUSIONS

This study undertook a comprehensive numerical investigation into the complex interplay of long-term subsidence and seismic loading on the performance of end-bearing pile foundations supporting a bridge structure using the direct approach to solve the soil-structure interaction problem within the challenging geotechnical context of Mexico City's basin. It will be important to complement the findings presented inhere with field measurements on bridges with emerging

issues due to ground subsidence. The simulations revealed that regional subsidence significantly impacts the static behavior of the foundation elements, generating down-drag forces on piles, detrimental gaps under footings, and surface cracking around structures. This last problem is often overlooked, since the bridge superstructure stability is prioritized over the adjacent infrastructure functionality, whose disruption can be manifested decades later (<20 years). As a result, less attention is paid by the current decision makers and stakeholders, who must demand that designers implement monitoring and mitigation strategies to prevent unexpected costly repairs.

Regarding the dynamic behavior associated to regional consolidation of the soil, the bridge´s deck Fourier spectra comparison reveals changes in frequency and amplification of the seismic motion as consolidation evolves. This amplification decreases, and the frequency where the main amplification occurs increases, linked to the loss of contact between the foundation and the soil, which changes drastically the way that the soil interacts with the structure, influencing the structure's overall vibrational response. To verify the impact at the foundation level, the footing base/free field transfer function was calculated, showing a reduction of the movement in all the frequencies in the consolidates cases, associated with loss of the footing-ground contact. Such results point out a change in the soil-foundation transfer mechanism of seismic motion, which occur mainly through the piles and lateral faces of the footings, in the consolidated cases.

This change is also reflected in the structural demand of the column and piles. In the time history analyses of the structure considering all consolidation stages, redistribution of seismic loads among the bridge could be observed as the subsidence progress. For the column's bending moments, the impact of regional subsidence was beneficial, with reductions of up to 75% for the 50 years condition. On the other hand, for the foundation, despite a reduction in the inertial movement of the superstructure, bending moments on the piles increased by up to 7 times their initial values after 50 years due to loss of soil confinement, which shifts most of the horizontal seismic demand to the piles.. Consequently, piles must be designed as short columns with significant transverse and longitudinal steel reinforcement, as required by some building codes worldwide, although this results in a costly solution.

With the findings gathered here, a deeper understanding of how regional subsidence impacts the long-term performance of bridge foundations was achieved

7 REFERENCES

AASHTO. 2023. *Guide Specifications for LRFD Seismic Bridge Design. 3rd ed.* Washington, DC: American Association of State Highway and Transportation Officials.

Abrahamson, N.A., 2000. Development of synthetic ground motions for seismic design. In: *Proceedings of the 6th International Conference on Seismic Zonation*, Palm Springs, California.

Barbosa, A.R., Mason, H.B., and Romney, K., 2014. *SSI-Bridge: Soil-Bridge Interaction during Long-Duration Earthquake Motions*. Report No. 2012-S-OSU-0008. Pacific Northwest Transportation Consortium.

Cabral-Cano, E., Solano-Rojas, D., Fernández-Torres, E.A. and Salazar-Tlaczani, L., 2024. Land subsidence hazards: A case study of Mexico City. In: *Remote Sensing for Characterization of Geohazards and Natural Resources*. Springer, 329–346.

Darendeli, M.B. and Stokoe, K.H., 2001. *Development of a new family of normalized modulus reduction and material damping curves*. Geotechnical Engineering Report GD01-12001. University of Texas at Austin.

FEMA. 2009. *NEHRP Recommended Seismic Provisions for New Buildings and Other Structures.* FEMA P-750. Washington, DC: Federal Emergency Management Agency.

Firoj M., and Maheshwari, B.K., 2022. Effect of CPRF on nonlinear seismic response of an NPP structure considering raft-pile-soil-structure-interaction. *Soil Dynamics and Earthquake Engineering*, 158, 102694.

Itasca Consulting Group, Inc. 2009. *FLAC3D – Fast Lagrangian Analysis of Continua in 3 Dimensions: User's Guide*. Minneapolis, MN: Itasca Consulting Group.

Lilhanand, K. and Tseng, W.S., 1988. Development and application of realistic earthquake time histories compatible with multiple damping response spectra. In: *Proceedings of the 9th world conference on earthquake engineering,* Tokyo, Vol. II., 819–24.

Lysmer, J., and Kuhlemeyer, R.L. 1969. Finite dynamic model for infinite media. *Journal of Engineering Mechanics Division*, 95(4), 859–878.

Mayoral, J.M., Castañon, E., and Albarran, J., 2017. Regional subsidence effects on seismic soil-structure interaction in soft clay. *Soil Dynamics and Earthquake Engineering*, 103, 123–140.

Mayoral, J.M., Romo, M.P., Mendoza, M.J., and Alberto, Y., 2009. Seismic response of an urban bridge-support system in soft clay. *Soil Dynamics and Earthquake Engineering*, 29(5), 925–938.

Mittal, V., and Samanta, M., 2021. A critical review on design philosophies of different design standards on seismic soil–structure interaction. In: *Proceedings of 7th International Conference on Recent Advances in Geotechnical Earthquake Engineering and Soil Dynamics*, 1-13.

Schanz, T., 1999. Formulation and verification of the Hardening-Soil Model. In: *Beyond 2000 in Computational Geotechnics*, 281-290.

Schnabel, P.B., Lysmer, J., and Seed, H.B., 1972. *SHAKE: a computer program for earthquake response analysis of horizontally latered sites.* Report No. EERC 72-12. University of California, Berkeley.

Seed, H.B. and Idriss, I.M., 1970. *Soil moduli and damping factors for dynamic response analyses*. Report No. EERC 70-10, Earthquake Engineering Research Center, University of California, Berkeley.

Singh, S.K., Reinoso, E., Arroyo, D., Ordaz, M., Cruz-Atienza, V.M., Pérez-Campos, X., Iglesias, A., and Hjörleifsdóttir, V. 2018. Deadly intraslab Mexico earthquake of 19 September 2017 (Mw 7.1): Ground motion and damage pattern in Mexico City. *Seismological Research Letters*, 89(6), 2272–2282.

O'Riordan, N., Basile, F., and Poulos, H.G., 2018. Negative skin friction and axial load implications for deep foundations in seismic zones. *Proceedings of the 7th International Conference on Earthquake Geotechnical Engineering*, Rome, Italy, 17–20 June 2019.

Osorio, L., and Mayoral, J.M., 2013. Seismic microzonation for the northeast Texcoco lake area, Mexico. *Soil Dynamics and Earthquake Engineering*, 50, 1–14.

Ovando-Shelley, E., Ossa, A., and Romo, M.P. 2007. The sinking of Mexico City: Its effects on soil properties and seismic response. *Soil Dynamics and Earthquake Engineering*, 27(4), 333–343.

RCDF (Reglamento de Construcciones para el Distrito Federal). 2023. *Gaceta Oficial de la Ciudad de México*, (in Spanish).

Wood, C.M., Woodfield, L.J., Rahimi, S., Rosado-Fuentes, A., Sánchez-Sesma, F.J., Cruz-Jiménez, H., Mayoral, J.M. and de la Rosa D., 2023. Shear wave velocity and site period measurements for the western portion of the Mexico City Basin following the Mw7.1 2017 Puebla–Morelos, Mexico, earthquake. *Earthquake Spectra*, 39(1), 505–527

Yeganeh, N., Bolouri, J., and Akhtarpour, A. 2015. Seismic analysis of the soil–structure interaction for a high rise building adjacent to deep excavation. *Soil Dynamics and Earthquake Engineering*, 79, pp. 149–170.

Zhao, M., Gao, Z., Wang, L., Du, X., Huang, J., and Li, Y. 2017. Obliquely incident earthquake for soil-structure interaction (SSI) in layered half space. *Earthquakes and Structures*, 13(6), 573–588.

Zúñiga, F.R. and Suárez, G., 2017. A first-order seismotectonic regionalization of Mexico for seismic hazard and risk estimation. *Journal of Seismology*, 21(6). 1295–1322